Foam flow in a model porous medium
I. the effect of foam coarsening

Jones, S. A.; Getrouw, N.; Vincent-Bonnieu, S.

DOI
10.1039/c7sm01903c

Publication date
2018

Document Version
Accepted author manuscript

Published in
Soft Matter

Soft Matter

ARTICLE

Foam Flow in a Model Porous Medium : I. The Effect of Foam Coarsening

Received 00th January 20xx,
Accepted 00th January 20xx

DOI: 10.1039/x0xx00000x

www.rsc.org/

S.A. Jones,[a,b,†] N. Getrouw[b] and S. Vincent-Bonnieu[b,c]

Foam structure evolves with time due to gas diffusion between bubbles (coarsening). In a bulk foam, coarsening behaviour is well defined, but there is less understanding of coarsening in confined geometries such as porous media. Previous predictions suggest that coarsening will cause foam lamellae to move to low energy configurations in the pore throats, resulting in greater capillary resistance when restarting flow. Foam coarsening experiments were conducted in both a model-porous-media micromodel and in a sandstone core. In both cases, foam was generated by coinjecting surfactant solution and nitrogen. Once steady state flow had been achieved, the injection was stopped and the system sealed off. In the micromodel, the foam coarsening was recorded using time-lapse photography. In the core flood, the additional driving pressure required to reinitiate flow after coarsening was measured. In the micromodel the bubbles coarsened rapidly to the pore size. At the completion of coarsening the lamellae were located in minimum energy configurations in the pore throats. The wall effect meant that the coarsening did not conform to the unconstricted growth laws. The coreflood tests also showed coarsening to be a rapid process. The additional driving pressure to restart flow reached a maximum after just 2 minutes.

Introduction

Gas injection has been used in the petroleum industry as an enhanced oil recovery technique since the 1930s. However, the sweep efficiency of the injected gas can be reduced by gravity override and viscous fingering, caused by the low density and viscosity of the gas. Using foam, where the gas exists in bubbles separated by liquid films instead of a single phase gas, as a fluid for Enhanced Oil Recovery (EOR) can overcome these obstacles. The main effect of the foam is to trap gas in the porous media, increasing the apparent viscosity and diverting the flow to the unswept zone. It is important to understand how the foam moves through the rock in order to predict behaviour during EOR processes. The structure of foam can change due to three phenomena: 1) the drainage of the liquid through film, which is neglected at the pore scale, 2) the film collapse, due to oil effect or capillary pressure and 3) coarsening, due to gas diffusion between bubbles.

This work focusses on the coarsening phenomena, also known as Ostwald ripening, in porous media. In particular, the way in which the structure of the foam evolves with time due to gas diffusion between bubbles and the effect of this on the foam flow behaviour. Although foam coarsening is well described in bulk foam, very few experiments have been carried out to study the coarsening in porous media[1]. In this work, coarsening experiments have been performed at both pore and core-plug scales. A glass micromodel allowed direct visualisation of the foam evolution at the pore scale, while coreflood experiments in outcrop sandstone samples were used to study the bulk coarsening behaviour at the Darcy scale (i.e. over a few cms).

Coarsening is driven by the pressure difference between two neighbouring bubbles, with gas diffusing from the higher pressure bubble to the lower pressure bubble at a rate determined by Fick's law[2] :

Rate of gas transfer across lamella = - mass transfer coefficient × film area × pressure difference. (1)

For a two dimensional foam, any liquid film between two bubbles has a radius of curvature, *r*, dependent on the pressure difference, ΔP, between the two bubbles. The pressure difference can be defined as:

$$\Delta P = 2\gamma/r \quad (2)$$

where γ is the surface tension of the liquid[3].

In a perfectly monodisperse two dimensional foam, all the bubbles have 6 sides and the internal pressure is constant for every bubble. In a polydisperse two dimensional foam, the smaller bubbles typically have fewer sides (<6) and higher pressures, and the larger bubbles have more sides (>6) and lower pressures[3]. Gas diffusion is then in the direction from the smaller bubbles to the larger bubbles, with the consequence that the smaller bubbles disappear completely. Von Neumann's law for a two dimensional foam[4] describes

[a] *Technical University of Denmark.*
[b] *TU Delft.*
[c] *Shell Global Solutions Int. B.V.*
† Corresponding author.

how the area, A, of a bubble varies with time as a function of the number of neighbours, *n*, and the permeability constant, κ.

$$\frac{dA}{dt} = \frac{2\pi}{3}\gamma\kappa(n-6) \quad (3)$$

Von Neumann's law predicts, and experiments have shown, that the average bubble area, <*A*>, increases linearly with time[3,5,6]. Correspondingly, the ratio $N_o/N(t)$, where N_o is the initial number of bubbles and $N(t)$ is the number of bubbles at time *t*, also increases linearly with time[7]. However, these relations are only valid when there is no boundary (wall) effect and for the case of a dry foam, where the meniscus between the lamella and the plates containing the 2D foam is neglected.

Coarsening behaviour in a bulk foam has been well defined[8]. However, there is still a lack of understanding of coarsening behaviour in confined geometries, especially in porous media. Foam in a porous medium coarsens quite differently than foam in bulk due to the geometric constraints of the pore walls[2]. The curvature of any lamellae within a porous media is determined both by the local geometry of the pore and by the fact that a lamella will always connect with the walls at 90°. As coarsening progresses, the lamellae rearrange and move to achieve a minimum energy configuration (Figure 1). Cohen et al.[2] found that once the system reaches equilibrium, the lamellae all rest in the pore throats where they have no curvature. There is thus no pressure drop across these lamellae, the pressure in the system will be uniform, and this configuration is thus indefinitely stable.

Numerical and analytical work by Nonnekes et al.[9] predicted that coarsening causes the foam lamellae to move to minimum energy configurations in the pore throats. Once the lamellae are in these locations the authors predicted that the films would give a greater capillary resistance when any attempt was made to restart flow.

The micromodel is a useful tool for mimicking porous media[10,11,12], representing, in two dimensions, channels, pore throats and pore bodies. The water saturation, bubble coarsening and the gas trapping can be easily monitored, via images of the bubbles, as function of time. However, the depth of the micromodel is constrained by the manufacturing technique, and the two dimensional geometry deforms the bubbles, making it difficult to give an exact comparison with three dimensional experiments.

Micromodels have been used to study foam coarsening because they give direct access to the microstructure of the foam[13,14] and the wettability can be changed to mimic the rock properties. Marchalot et al.[7] also carried out coarsening experiments in a microfluidic set-up, but this was effectively a bulk foam test as the effect of the walls were minimised.

In this work, coarsening was studied using a 2D micromodel to monitor the bubble size evolution and the positions of the bubble films. The results were compared to coreflood experiments in rock, where a "restart" pressure drop, indicative of the increased capillary resistance postulated by Nonnekes et al.[9], was measured after the foam had been allowed to coarsen for a certain time.

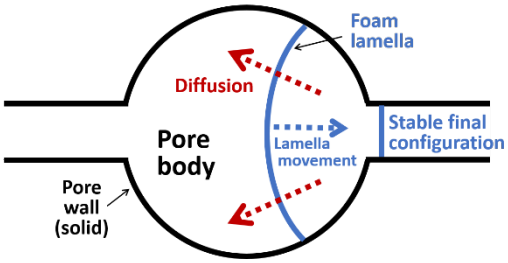

Figure 1 Sketch of diffusion process in a pore. The local curvature of the lamella is determined by the local geometry of the pore. The diffusion results in a final, minimum-energy configuration of the lamella in the pore throat.

Experimental Method

Micromodel Tests

Foam coarsening tests were carried out in a borosilicate-glass 2D micromodel. The micromodel was etched with an irregular hexagonal pattern that formed a model porous medium, with a Gaussian distribution of pore diameters (mean = 60 µm) and throat widths (mean = 13 µm) (Figure 2). The pattern had a total width of 800 µm (10/11 pores) and an overall length of 60 mm (849 pores), with a channel depth of 5 µm. The porosity of the micromodel, ϕ = 0.77, was calculated from the pore pattern, and the permeability was measured to be 0.72 D.

Surfactant solution and nitrogen gas were co-injected into the micromodel through a frit, with 10 µm pores, to generate a foam with quality of 0.98. The surfactant used was a Sodium C14-16 Alpha Olefin Sulfonate (AOS) (Bioterge AS-40K), a surfactant commonly used in foam core floods for Enhanced Oil Recovery (EOR) research, and the solution contained 0.5 wt% total active surfactant in demineralized water. The surfactant solution was injected using a syringe pump fitted with a 20 ml stainless steel syringe, which was capable of a flow rates as low as 0.25 $\mu L.min^{-1}$ (equivalent to a superficial velocity of 1.04 x 10^{-3} ms^{-1}). The gas injection was controlled using a mass flow controller with a full scale of 0.7 $ml.min^{-1}$. The pressure in the system was monitored using two absolute pressure transducers (60 bar full-scale, ±0.04% FS).

Once steady state foam flow was achieved in the micromodel, with a relatively stable pressure drop across the model indicating that no major foam evolution was occurring, the flow was stopped and the micromodel sealed off. The

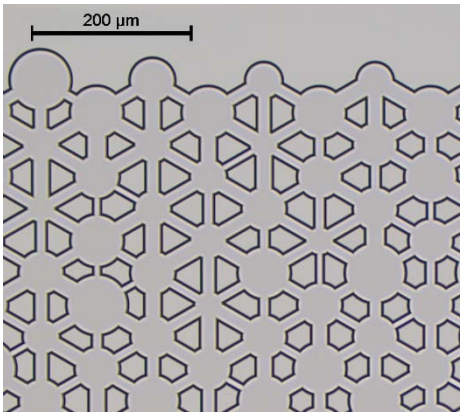

Figure 2 Photograph of a section of the micromodel, showing the distribution of pore diameters and pore throat widths.

coarsening behaviour of the foam midway along the micromodel was then observed. This imaging location was chosen to ensure that the observed foam was well established and to avoid any potential entrance or end effects. The foam was observed using an inverted microscope (Leica DMi8) in Transmitted Light mode, with a X10 objective that allowed the whole width of the porous channel to be viewed. Images of the micromodel, and the foam within the pores, were recorded using a high-resolution video camera connected to the microscope. This camera had a resolution of 1920x 1440 pixels and could either be used to record video at 6 frames per second, or to take time-lapse photographs at user defined intervals over extended periods of time. The images of the foam were then processed and binarised using the ImageJ software package[15] before analysis of the bubble sizes.

Core Flood

Coarsening experiments were also carried out in a Bentheimer sandstone outcrop core, with a porosity, ϕ, of 0.23 and permeability of 0.88 D. The core had a diameter of 1 cm and a length of 17 cm, as previously described in Jones et al.[16]. Pressure measurements were made at four locations along the core, as indicated in the schematic diagram of the core-flood set-up (Figure 3), and the back pressure was set at 20 bar. Foam was produced by co-injecting surfactant solution and nitrogen at the base of the core, with a total flow rate of 0.1 ml.min^{-1} and a foam quality of 0.5. Once a steady state flow was achieved, the flow was stopped and the core sealed off. After a fixed coarsening time, t_c, the flow was restarted, and the pressure was monitored closely during the reinitiation of flow. It is assumed that coarsening is the only mechanism in place during the stoppage time, and any additional driving pressure required to reinitiate flow could be attributed to the increased capillary resistance that results from the stable configuration of the coarsened foam[9]. It was, to our knowledge, the first time that this coarsening effect has been measured in a coreflood experiment.

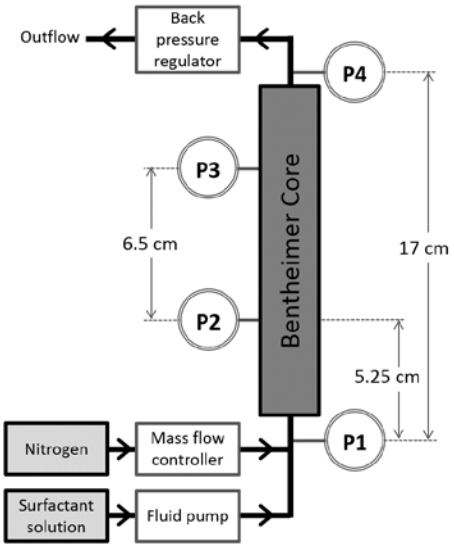

Figure 3 Schematic diagram of the core flood set-up, with the locations of the four pressure gauges indicated.

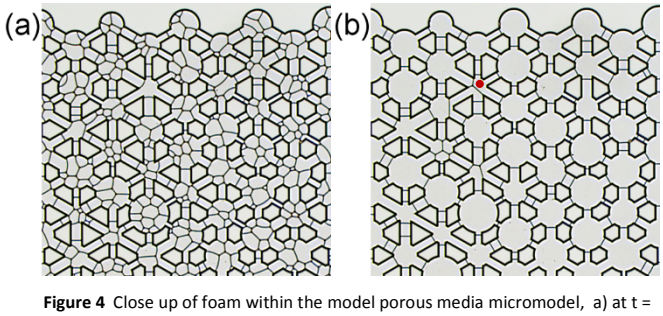

Figure 4 Close up of foam within the model porous media micromodel, a) at t = 0, before coarsening begins, and b) after 2000 seconds of coarsening. The foam has coarsened such that the majority of the bubble films are now located in minimum energy configurations in the pore throats. The red dot indicates a typical cross-pore stable configuration.

Results and Discussion

Micromodel Tests

Typical images of the foam in the micromodel, both before and after coarsening, are shown in Figure 4. It can be seen that the foam initially contained a wide distribution of bubble sizes, with a large proportion much smaller than the pore bodies. After 2000 seconds, diffusion between the bubbles had resulted in the majority of the lamellae residing in minimum energy configurations in the pore throats, apart from a few lamellae which maintained stable configurations across pores (example marked with red dot on Figure 4b). In our experiment, we never saw film coalescence, i.e. rupture. The only mechanism observed in the micromodel was coarsening by gas diffusion.

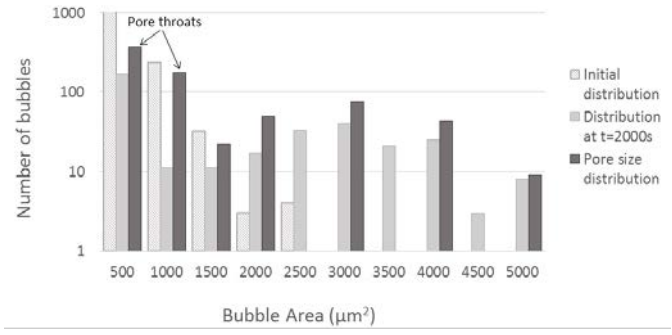

Figure 5 Bubble size distribution in the micromodel, both before coarsening and after 2000 seconds of coarsening, for a single coarsening test (representative of the general behaviour seen in repeat tests). The pore body and pore throat size distribution is included for comparison (the pore throat sizes are indicated, all other sizes are for pore bodies). The average pore diameter is 60μm, equivalent to an area of 2827 μm^2.

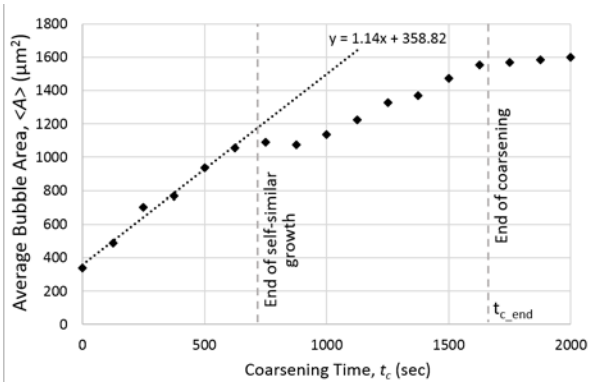

Figure 6 The average area of the bubbles, *<A>*, plotted as a function of the coarsening time, t_c, for a single coarsening test (representative of the general behaviour seen in repeat tests).

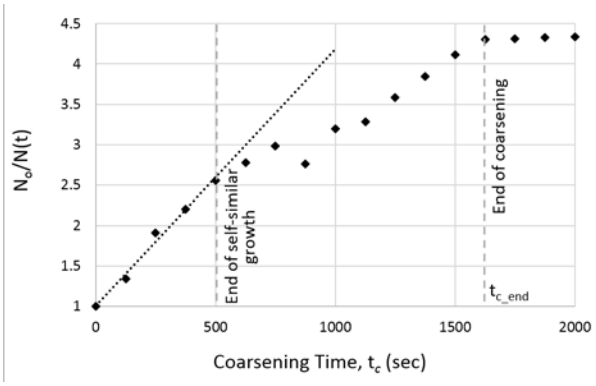

Figure 7 The ratio of the initial number of bubbles, N_o, to the number at time t_c, $N(t_c)$ plotted as a function of time, for a single coarsening test (representative of the general behaviour seen in repeat tests).. The experimental data deviates from the linear trend after approximately 500 seconds.

Considering the bubble size distribution (Figure 5), it can be seen that the initial foam had a predominance of bubbles much smaller than the pores (average bubble area, *<A>* = 383 μm^2). After 2000 seconds of coarsening, the bubble size distribution had evolved to a bimodal distribution. The first local maximum (at bin [1, 500] μm^2) represents the large number of small bubbles trapped in the pore throats, where the lamellae had no curvature and no further coarsening was possible. The second local maximum (at bin [2501, 3000] μm^2) represents the bubbles in the pore bodies that had coarsened to the pore size. The bubble size distribution above 1500 μm^2 closely matches the pore size distribution.

The average bubble area, *<A>*, was also measured as a function of the coarsening time, t_c (Figure 6). The average bubble area is expected to grow, due to coarsening, linearly as function of time (or the radius as a function of $t^{1/2}$)[3,6]. Our experiments confirmed that the bubbles initially grew linearly with time, with a gradient of 1.14 μm^2.s^{-1}. This value is significantly lower (by 2 to 3 orders of magnitude) than previous values of the gas diffusion coefficient measured without wall effect eg 128 μm^2.s^{-1} for a 2D micromodel foam[7] and 2000 μm^2.s^{-1} for a single bubble at the gas-water interface[17]. The significantly lower value of the diffusion coefficient in the current experiment reinforces the impact of the walls on coarsening in very confined geometries. It is remarkable that the bubble growth shows any linearity with time, as this is predicted for a 2D cell without boundary effects, and the current geometry should feel the effect of the boundaries very strongly. However, the initial foam structure (Figure 4a) shows many small bubbles within each pore, and thus the linear growth may be due to each pore exhibiting pseudo-bulk-foam behaviour.

The growth deviates from the linear after a relatively short time (~625 sec), as the effect of the confining pore walls on the coarsening becomes increasingly felt. Our experiment showed that the bubble films migrated to the pore throats (Figure 4b), and that the rate of coarsening decreased when the bubble size distribution became close to the pore size distribution. There is a corresponding decrease in the gradient of the average area curve above 625 seconds, and as the experiment progresses we can see that the value of the average bubble area tends towards a plateau value of ~1600 μm^2, at a time t_{c_end} of 1625 seconds. It was expected that the average bubble area would tend to the average pore size (2827 μm^2), but the large number of small bubbles trapped in the pore throats skews the average downwards.

Another characteristic of the coarsening is the ratio $N_o/N(t_c)$, the initial number of bubbles N_o to the number of bubbles at time t_c, $N(t_c)$ (Figure 7). Comparing with Figure 6, it is suggested that the consideration of $N_o/N(t_c)$ may be more sensitive to changes in behaviour than *<A>*, in a confined system, due to the discrete nature of the data (as opposed to the smoothing effect that occurs when averaging the area over a large number of bubbles). The outlier point observed at 875 seconds in Figure was caused by a pulse of residual flow, inevitable due to the pressure gradient that exists along the micromodel even after flow has stopped, that moved a number of smaller bubbles into the field of view.

Both the average bubble areas and $N_o/N(t_c)$ show three coarsening regimes:

1) The coarsening is initially self-similar[18], meaning that the topology of the bubble structures remains invariant with time. Linear growth of $N_o/N(t_c)$ is expected in this self-similar regime[19]. Linear growth with time is also characteristic of the coarsening when there are no boundary effects[7].
2) A deviation from the linear growth is an indication of when wall effects become significant. In this case, the boundary wall effect becomes noticeable after 500 seconds (end of self-similar growth indicated on Figure 7).

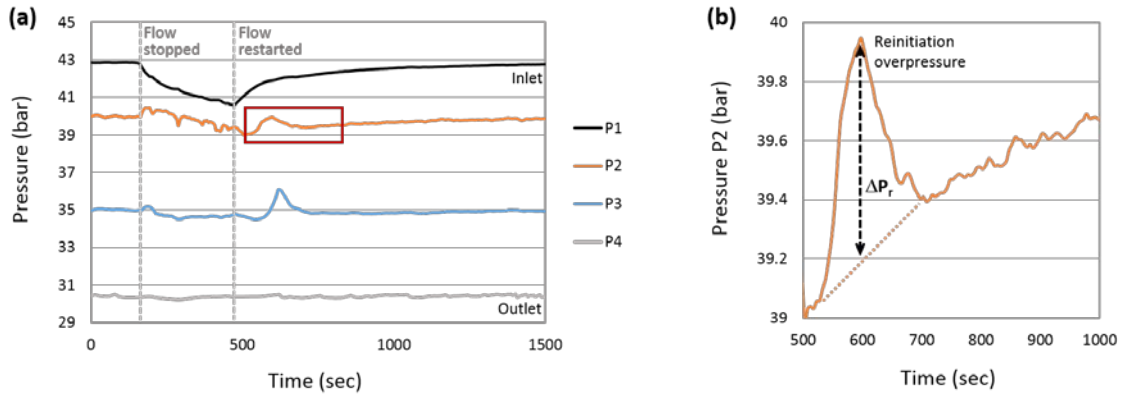

Figure 8 (a) Pressure measurements at the four locations along the core, showing the initial steady state flow, and the behaviour during both stoppage (t_c = 5 minutes) and flow reinitiation. (b) Close up of the pressure trace at P2 (red box). Assuming that the pressure trace without coarsening would follow the smooth increase indicated by the dashed orange line, we can then define the reinitiation overpressure, ΔP_r, caused by the coarsening of the foam (dashed black line).

3) Finally, the coarsening stops around 1600 seconds. The images (Figure 4b) show that at this time the majority of the foam films are sitting in the pore throats, and it appears that the bubbles are thermodynamically stable. The foam films have no curvature, meaning that the pressure drop between bubbles is nil, and consequently gas diffusion is expected to be limited. It is remarkable that the coarsening stops after less than one hour, as this means that the foam is expected to be stable on the longer time. One experiment was conducted over 3 days, showing no topological changes. It can be speculated that the foam structure would remain stable for longer time scales (days or weeks) but this needs to be verified in long duration experiments.

Core Flood

The pressure across the core was closely monitored both during the stoppage of the foam flow through the core and during the reinitiation of the flow. A typical pressure profile obtained during the flow stoppage and restart is shown in Figure 8a. The magnitude of the pressures, and the pressure drop along the core, are standard for the flow of foam through a Bentheimer core. As can be seen, once the flow is stopped there are some fluctuations in the measured pressure, and a noticeable drop in pressure at the inlet, due to residual flow driven by the pressure gradient along the core. In general, however, the pressures are remarkable stable, with the foam in the core minimising the amount of residual flow. Once flow restarts the pressures rise back to the original steady state values, but there is a distinct transient pressure peak at both the mid-core measurement locations (P2 and P3) just after the flow reinitiates. The existence of this pressure peak was suggested both by the theory and simulations of Nonnekes et al.[9] and by the current microfluidic experiments. In both these cases it was found that coarsening moves the lamella into very stable positions in the pore throats. When flow restarts, the lamellae therefore have to overcome a pressure barrier in order to move out of the pore throats, which thus increases the observed pressure drop.

Looking more closely at the reinitiation pressure peak for pressure gauge P2 (Figure 8b), we can consider how the pressure should change if there was no coarsening in the foam. It would be expected that, without coarsening, the pressure would rise smoothly to steady state values, as indicated by the dashed orange line in Figure 8b). We can then define a reinitiation overpressure, ΔP_r, (dashed black arrow) that results from the extra resistance to flow of the stable coarsened bubbles.

Flow stoppage tests were carried out for a range of coarsening times, with values of t_c between 10 seconds and 10 minutes. The reinitiation overpressure, ΔP_r , was measured at both of the mid-core locations (5.25 cm and 11.75 cm from the inlet), and the variation of ΔP_r with coarsening time is shown in Figure 9.

It can be clearly seen in Figure 9 that the coarsening process occurs very rapidly at the scale of the pores in Bentheimer sandstone, with an effect on the pressure seen after just 10 seconds of coarsening, with values tending towards a plateau of approximately 0.6 bar with increasing t_c. It is suggested that the coarsening stops (t_{c_end}) after less than 2 min.

Comparing these core flood tests with the micromodel tests, it can be seen that the coarsening stops much earlier in the coreflood (2 min) than in the micromodel (~25min). This disparity may be due to the differences between the structure

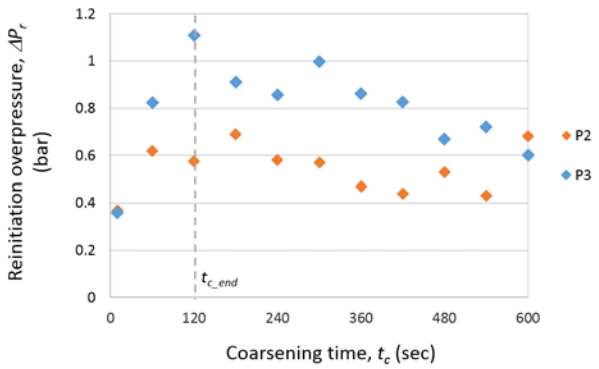

Figure 9 Reinitiation overpressure, ΔP_r , plotted as a function of the coarsening time, t_c , for the two mid-core pressure measurement locations.

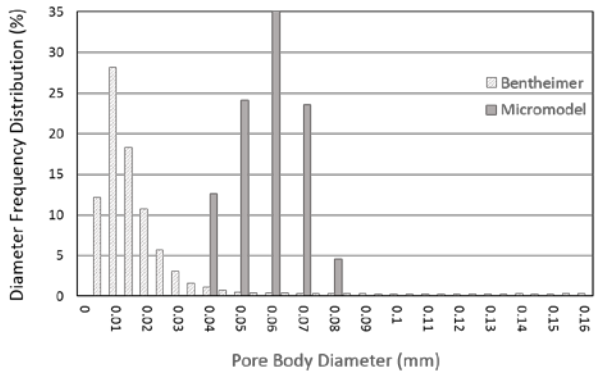

Figure 10 Frequency distribution of the pore body diameters for both the Bentheimer sandstone outcrop core (adapted from [20]) and the micromodel. The Bentheimer core contains a larger number of smaller pores than the micromodel, but also exhibits a much wider range of pore sizes.

of the rock and the micromodel. The pore size distribution is much wider in the rock[20], with a higher frequency of smaller pore bodies and throats (Figure 10, adapted from [20]). This results in the bubbles feeling the boundary constraints more rapidly in the rock than in the micromodel. Also, the roughness of the pore bodies is expected to be much greater in the real rock sample. The greater number of sharp edges found in the pores would create equilibrium configurations (or pinning locations) for lamellae. We can speculate that the number of stable configurations could be larger in the rock core than in our micromodel which could explain why the coarsening stops earlier.

The behaviour at P3 is unusual in that it exhibits a distinct maximum after just 2 minutes of coarsening time. It would be expected that once coarsening occurs, the overpressure will stay constant over t_c, but in this case, we have a maximum followed by a significant decrease in the value of ΔP_r before reaching the final value of 0.6 bar (Figure 9). The reason for this is currently not know. Bubble coalescence is not expected to have any effect at the time scales involved or to be so localised. It is possible that the behaviour is caused by the residual flow, but further experiments are required to clarify this issue.

It is noted that there are some differences between the coarsening behaviour at the two pressure locations, with the measurements closer to the core inlet showing smaller overpressures.. It is suggested that this is partly due to the effect of residual flow within the core. Considering the pressure traces in Figure 7a, it can be seen that the pressure at the location further from the inlet (P3 – blue curve) stabilises fairly quickly to a near constant value after the flow is stopped, giving a stable environment for coarsening to progress (and hence larger values of ΔP_r). In contrast the pressure closer to the inlet (P2 - Figure 7a, orange curve) continues to drop, with noticeable fluctuations, for the whole 5 minutes of flow stoppage. The residual flow that would accompany these changes in pressure could disrupt the coarsening, as observed in the micromodel, resulting in the smaller overpressures observed. The effect of this transient behaviour lasts for approximately 8 - 10 minutes, when the behaviour at the two locations converges at $\Delta P_r \approx 0.6$ bar.

Conclusions

The coarsening behaviour of foam has been investigated, both at the pore scale, in a 2D micromodel, and at the core scale. There was a difference between the coarsening time scales at the pore scale and the core scale.

The specific observations made in the 2D micromodel and in the core flood tests are as follows:

- The 2D micromodel is particularly useful in the study of foam coarsening behavior, as it can provide detailed information on the changing structure of the foam, including bubble size and lamella location.
- Three coarsening regimes were observed in the micromodel experiments: 1) a self-similar regime with a linear growth of the average bubble size with time; 2) a decrease of the coarsening rate, where the constraint of the boundary limits at the walls becomes significant; 3) the coarsening ends after about 25 min with the majority of bubbles films sitting in the pores throats.
  - The average bubble areas, $\langle A \rangle$, initially varied linearly as function of time (regime 1). The slope of the line started falling after 625 seconds, indicating that the effect of the pore walls was becoming more dominant (regime 2).
  - The $N_o/N(t_c)$ graph also provided a good indication of when the confining pore walls began to have a significant effect on the coarsening behavior of the foam (regime 2).
  - The final bubble size distribution tended to a bimodal distribution, indicating the large number of small bubbles trapped in the narrow pore throats, and the bubbles in the pore bodies that had coarsened to the pore size (regime 3).
- The coreflood experiments showed that, as previously predicted[9], a coarsened foam provides an extra capillary resistance to flow in a porous media. This results in the excess pressure required to restart the foam flow, the reinitiation overpressure, ΔP_r.
- The coarsening behavior in the Bentheimer sandstone is relatively rapid, as compared to the micromodel tests, with an effect being observed after just 10 seconds of stopped flow and with a maximum value of ΔP_r being observed after just 2 minutes of coarsening time. The coarsening was observed to stop much earlier in the rock than in the micromodel, possibly because the pores and pore throats are smaller in the sandstone than in the micromodel.

Conflicts of Interest

There are no conflicts of interest to declare.

Acknowledgements

We would like to acknowledge the financial support from Shell Global Solution International B.V., the technical support of Michiel Slob, and useful discussions with Dr. Evren Unsal.

Notes and references

1 B. Géraud, S.A. Jones, I. Cantat, B. Dollet and Y. Méheust, *Water Resources Research*, 2016, **52**, 773–790.
2 D. Cohen, T. Patzek, and C. Radke, *Journal of Colloid and Interface Science*, 1996, **373**, 357–373.
3 D. Weaire and S. Hutzler, *The Physics of Foams*, Clarendon Press, Oxford, 1999.
4 J. Von Neumann, in *Metal interfaces,* American Society for Metals, Cleveland, 1952, 108-110.
5 J. Stavans, *Physical Review A*, 1990, **42**, 5049-5051.
6 P. Stevenson (Ed.), *Foam engineering: Fundamentals and applications*, John Wiley and Sons, 2012.
7 J. Marchalot, J. Lambert, I. Cantat, P. Tabeling and M.-C. Jullien, *EPL*, 2008, **83**, 64006.
8 J.A. Glazier, S.P. Gross and J. Stavans, *Physical Review A*, 1987, **36**, 306-312.
9 L.E. Nonnekes, S.J. Cox, and W.R. Rossen, *Transport in Porous Media*, 2015, **106**, 669-689.
10 K. Ma, R. Liontas, C.A. Conn, G.J. Hirasaki and S.L. Biswal, *Soft Matter*, 2012, **8**, 10669–10675.
11 M. Robin, J. Behot and V. Sygouni, *Proceedings of SPE Improved Oil Recovery Symposium*, 2012, **2**, 1–15.
12 D. Manlowe and C. Radke, *SPE Reservoir Engineering*, 1990, **5**, 495–502.
13 L. Romero-Zeron and A. Kantzas, *Journal of Canadian Petroleum Technology*, 2005, **44**, 44-50
14 L. Romero-Zeron and A. Kantzas, *Journal of Canadian Petroleum Technology*, 2006, **45**, 51-62
15 W.S. Rasband, ImageJ, U. S. National Institutes of Health, Bethesda, Maryland, USA, http://imagej.nih.gov/ij/ , 1997-2016
16 S.A. Jones, V. van der Bent, R. Farajzadeh, W.R. Rossen and S. Vincent-Bonnieu, *Colloids and Surfaces A: Physicochemical and Engineering Aspects*, 2016, **500**, 166-176.
17 H.M.Princen, J.Th.G. Overbeek and S.G. Mason, *Journal of Colloid and Interface Science*, 1967, **24**, 125-130
18 J. Lambert, R. Mokso, I. Cantat, P. Cloetens, J.A. Glazier, F. Graner and R. Delannay, *Physical Review Letters*, 2010, **104**, 248304.
19 J. Stavans, *Reports on Progress in Physics*, 1993, **56**, 733-789.
20 A.E. Peksa, K.H.A. Wolf and P.L. Zitha, *Marine and Petroleum Geology*, 2015, **67**, 701-719.